Macromolecules

ARTICLE

pubs.acs.org/Macromolecules

Interface of Grafted and Ungrafted Silica Nanoparticles with a Polystyrene Matrix: Atomistic Molecular Dynamics Simulations

Tinashe V. M. Ndoro,*[,†] Evangelos Voyiatzis,[‡] Azadeh Ghanbari,[†] Doros N. Theodorou,[‡] Michael C. Böhm,[†] and Florian Müller-Plathe[†]

[†]Eduard-Zintl-Institut für Anorganische und Physikalische Chemie, Technische Universität Darmstadt, Petersenstrasse 20, D-64287 Darmstadt, Germany

[‡]School of Chemical Engineering, National Technical University of Athens, 9 Heroon Polytechniou Street, Zografou Campus, GR-15780, Greece

Supporting Information

ABSTRACT: Atomistic molecular dynamics simulations of a composite consisting of an ungrafted or a grafted spherical silica nanoparticle embedded in a melt of 20-monomer atactic polystyrene chains have been performed. The structural properties of the polymer in the vicinity of a nanoparticle have been studied. The nanoparticle modifies the polymer structure in its neighborhood. These changes increase for higher grafting densities and larger particle diameters. Mass and number density profiles show layering of the polymer chains around the nanoparticle, which extends to ∼2 nm. In contrast, the increase in the polymer's radius of gyration and other induced ordering (alignment of the chains parallel to the surface and orientation of backbone segments) are shorter-ranged. The infiltration of free polystyrene chains into the grafted chains region is reduced with increasing grafting density. Therefore, the interpenetration of grafted and free chains at high grafting densities, which is responsible for the mechanical anchoring of nanoparticles in the polystyrene matrix, is less than what would be desirable for a well-reinforced composite.

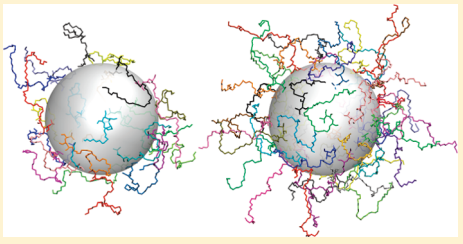

1. INTRODUCTION

Composites of inorganic particles embedded in a polymer matrix have attracted scientific and technological attention for a variety of reasons. For example, the rubber industry widely employs carbon black and silica particles of a wide size distribution as reinforcing fillers.[1,2] Carbon black increases tire strength and toughness while also improving the rubber's resistance to tearing, abrasion, and flex fatigue.[3,4] Consequently, the traction of rubber and its durability are increased. It is therefore possible and advantageous to combine the properties of different materials, for example, elastomers or rubber with carbon black or silica, to make functional materials where one component provides the function and the other the mechanical strength. The usage of nanoparticles as additives to modify polymer properties has greatly increased with many different possibilities being explored.[5,6] In most cases, a regular dispersion of the nanoparticles in the polymer is desired to prevent particle aggregation.[6,7] This can be achieved by compatibilizing the nanoparticle and polymer, for example, by coating the nanoparticle or grafting it with a polymer.[8] Such polymer brushes are also used for other physicochemical applications such as colloid stabilization[9] and dispersion[10] or improved lubrication.[11,12] It has been observed by Mackay et al.[13] that the addition of nanoparticles to polymer melts can lead to a non-Einstein-like decrease in the viscosity. This can be employed to lower the viscosity of polymers for processes such as extrusion and injection-molding without compromising the mechanical strength of the final object.

An important part of a composite is the interface between the polymer and inorganic filler. The mere existence of the interface modifies the polymer structure.[14] The structural perturbation can extend to more than just the first molecular layer and can cause the formation of an interphase where the polymer does not (yet) show bulk-like behavior. This phenomenon is particularly pronounced for nanocomposites. In the nanometer-size interstices between nanoparticles, the polymer will not always reach its bulk behavior. Structural modifications are expected for both bare and grafted nanoparticles, but they will be different. As a result of their unusual properties, polymer interfaces formed near solid surfaces have attracted considerable interest from both academic and industrial communities. For example, Tsagaropoulos et al.[15] observed that many polymer properties such as viscosity, diffusion coefficient, or the T_2 relaxation time in NMR measurements dramatically change in the interfacial region. These differences are attributed to restrictions on the mobility of polymer chains in the vicinity of a surface. The reduced mobility has, in turn, been explained by a decrease in the configurational entropy due to crowding, ordering at the interface, or both.

The polymer nanocomposites studied in this work consist of either an ungrafted or a grafted spherical silica nanoparticle of varying diameters and surrounded by a polystyrene matrix. The interaction between grafted and free chains on one hand and with the surface on

Received: December 13, 2010
Revised: January 26, 2011
Published: March 08, 2011

the other hand determines the dispersion state of the nanoparticles and whether reinforcement is improved. Recent experimental work by Chevigny et al.[16,17] has shown that these interactions are one of the key factors in controlling the dispersion of nanoparticles. Dispersion of nanoparticles into polymeric matrices remains an outstanding problem, as highlighted in the recent review article of Kumar and Krishnamoorti.[18] To control polymer dispersion, understanding of the factors involved in the interaction between grafted and free chains is vital. The free energy of swelling polymer brushes consists of a mixing entropy term between the grafted and ungrafted chains and an elastic deformation term for the grafted chains. Entropic effects drive the chain interpenetration and scale inversely with the molecular weight. Borukhov et al.[19] also introduced an enthalpic interaction term to explain the mixing of large solvent molecules with polymer brushes.

Following this short overview of experimental activities, we will now comment on simulation studies performed on polymeric nanocomposites. There are many studies of ungrafted nanoparticles in polymers at various levels of theory. Frischknecht et al.[20] employed a coarse-grained (CG) variant of the self-consistent polymer reference interaction site model (SC/PRISM) to study the effect of well-dispersed nanoparticles on the equilibrium chain configurations. They observed an expansion in the polymer radius of gyration, R_g, when the nanoparticle radius was below R_g. This effect was further enhanced with increasing nanoparticle volume fraction. Chain expansion was suggested to be a result of both the excluded volume taken up by the nanoparticles and the attractive interaction between the monomers and the nanoparticles. Both phenomena make the nanoparticles behave like a good solvent. Polymer chains formed bound layers around multiple nanoparticles, and their packing changed over a length scale up to three nanoparticle diameters.

Also employing the PRISM theory, Hooper and Schweizer[21,22] sought to identify "design rules" for the thermodynamic stability and miscibility of fillers in dense polymer melts. In their work, they reported that the particle−particle potential of mean force can show contact aggregation, steric stabilization, local bridging attraction, and longer range "tele-bridging" attraction. This behavior depends on the strength and spatial range of intermolecular attractions. The observed steric stabilization of the spherical particles is attributed to the thermodynamic stability of distinct bound polymer layers. This knowledge can assist in the rational design to achieve good particle dispersion and thus homogeneous mixtures.

Using Monte Carlo (MC) simulations of a coarse-grained model, Vogiatzis et al.[23] investigated the structure of a polystyrene matrix filled with an ungrafted nanoparticle, made up of internally tightly cross-linked polystyrene. Their work shows an increased polymer density near the nanoparticle surface. The calculated density profiles were only weakly dependent on the chain length. The authors furthermore reported that interfacial chains orient with their longest dimension tangentially to the nanoparticle surface. Similar observations were seen for local chain segments.

Fully atomistic molecular dynamics (MD) simulations of an ungrafted spherical silica nanoparticle embedded in a poly(ethylene oxide) (PEO) matrix by Barbier et al.[24] revealed dense packing of flattened PEO backbones arranged in ordered shells around the nanoparticle. Interactions between PEO and silica further stabilized the densely packed shells. Analogous to the work of Vogiatzis et al.,[23] they observed two distinct density maxima near the nanoparticle surface. This well-defined layering effect is typical of strongly attractive polymer−surface interactions. The predicted alignment of the PEO backbones parallel to the silica surface was strongest in the first layer. Note that these results are similar to observations of a generic polymer in the vicinity of a surface.[25] The increase in the polymer density near the surface was also reported by Borodin et al.,[26] who studied the interface between PEO and a planar crystalline TiO_2 surface.

Computer simulation work of polymer composites containing ungrafted surfaces has also been carried out in our group. In these studies, however, the surfaces were flat; that is, they are representative of large filler particles (particle curvature radius is large compared with the polymer radius of gyration). Eslami and Müller-Plathe[27] performed atomistic MD simulations of polyamide-6,6 trimers confined between graphite surfaces. They observed a layering/structuring effect of the oligomers parallel to the surface. Recent work on the structural properties of polyamide-6,6 tetramers around one and two embedded carbon nanotubes (CNTs) also reveals dense chain packing around the CNT surface.[28]

There is also a considerable body of simulation work on polymer-grafted surfaces and nanoparticles. Grest[29] pioneered computer simulations of a polymer brush in a polymer melt. Previous work had only simulated polymer brushes in solvents. The challenge of simulating a polymer melt is that most of the computer time is spent calculating the melt and not the brush. Both MD and MC studies of a system of chains attached to a flat surface demonstrated that the brush height at low coverage is nearly independent of the grafting density (ρ_{gr}, chains per surface area, i.e., chains/nm^2). At higher surface coverage, it increases as $(\rho_{gr})^{1/3}$. Layering of monomers close to the surface was evident in both the overall number density and the brush monomer number density. The number of free chains that were excluded from the brush volume increased with increasing chain length because of entropic interactions and excluded volume effects, showing a crossover from a wet to a dry brush.

Lo Verso et al.[30] compared MD and density functional theory (DFT) to study a coarse grained model of fully flexible polymers end-grafted to repulsive spherical nanoparticles under good solvent conditions. In their systems, R_g is similar to the size of the nanoparticle. The density profiles for both methods show a tightly bound monolayer close to the surface that is followed by a clearly visible second layer. They report a local stretching of the grafted chains and a decrease in the tangential orientation to the surface with increasing ρ_{gr}. However, their DFT method overestimated chain stretching with increasing surface curvature.

In the entanglement regime, Kalb et al.[31] analyzed the effect of surface coverage and curvature of spherical grafted nanoparticles on the autophobic dewetting of the melt from the brush. Using MD, they employed a coarse-grained bead−spring model with a truncated and shifted Lennard-Jones potential for brush and melt monomers. These authors integrated this potential over the nanoparticle sphere to obtain the interaction between the nanoparticle and the brush as well as the melt monomers. Their work shows that the solvent quality of the melt becomes progressively poorer with increasing ρ_{gr}. It becomes increasingly more difficult to compensate for the entropic loss upon brush infiltration of the matrix chains. In addition, polymer brush chains attached to small nanoparticles of higher curvature can explore more space. The opposite is true for chains attached to a planar surface. Consequently, this results in a greater entropic loss for matrix chains wanting to infiltrate. The radial brush monomer density profiles changed from concave for small nanoparticles (behavior similar to star polymers) to parabolic for large particles.

Lattice MC simulations on a system of linear chains end-grafted to a spherical surface were performed by Klos and Pakula[32−34] using the cooperative motion algorithm. The monomer concentration profiles under good solvent conditions are reported to change from concave to convex with increasing nanoparticle radius. For small surface coverage, a depletion layer is observed for the latter. In the case of

Table 1. Studied Nanocomposite Systems (T = 590 K, P = 101.3 kPa)

number of grafted a-PS chains	number of free a-PS chains	ρ_{gr}/chains/nm^2	mass density/kg/m^3	SiO_2 core/mass%	grafted a-PS chains/mass%	free a-PS chains/mass%	simulation time/ns	box length/nm
			Nanoparticle Diameter ∅ = 3 nm					
0	202	0.0	940.11 ± 0.87	5.3	0.0	94.7	73.1	9.23 ± 0.01
14	188	0.5	948.00 ± 0.83	5.3	7.2	87.5	68.1	9.23 ± 0.01
28	174	1.0	944.71 ± 0.56	5.3	14.2	80.5	66.0	9.26 ± 0.01
			Nanoparticle Diameter ∅ = 4 nm					
0	202	0.0	980.91 ± 0.90	11.7	0.0	88.3	64.0	9.31 ± 0.01
25	202	0.5	976.52 ± 1.09	11.7	9.5	78.8	57.0	9.69 ± 0.01
50	177	1.0	978.10 ± 0.87	11.7	20.0	68.3	47.6	9.71 ± 0.01
			Nanoparticle Diameter ∅ = 5 nm					
0	202	0.0	1042.70 ± 0.35	20.5	0.0	79.5	63.1	9.46 ± 0.01
40	162	0.5	1046.80 ± 1.32	20.5	16.8	62.7	50.7	9.49 ± 0.01
80	122	1.0	1047.46 ± 1.27	20.5	33.0	46.5	50.0	9.54 ± 0.01

small ρ_{gr} (surface coverage) and particularly for smaller nanoparticles with a high curvature, chain centers of mass were found inside the particle, indicating that the polymers can wrap around it. Similar observations have been reported by Vogiatzis et al.[23] Chains near the surface were tangentially oriented to it, whereas distant chains had stronger radial orientations.

Cordeiro et al.[35] investigated the mutual repulsion of two PEO-grafted surfaces by a combination of atomistic and coarse-grained models. Repulsive surfaces made chains to attain more extended conformations, whereas chains adsorbed onto attractive surfaces. They observed that the chain length had a larger influence on the particle stability when comparing particles of similar grafting density but different chain molecular weight.

Trombly and Ganesan[36] have employed the polymer mean-field theory to study curvature effects of polymer-grafted nanoparticles immersed in a chemically identical polymer melt. The interpenetration width between grafted and free chains was quantified as a function of surface curvature, grafting density, and the relative molecular weights of the grafted and free chains. The stretching cost of the grafted chains associated with the penetration of free chains was found to reduce with increasing surface curvature, thereby enhancing the tendency for interpenetration of free chains into the grafted chains regime.

To understand better the structural properties of a chemically realistic polymeric matrix around spherical nanoparticles, we have used MD simulations to study an atactic polystyrene (a-PS) matrix surrounding either an ungrafted or a grafted spherical silica nanoparticle. We have performed these simulations as a function of the nanoparticle curvature, that is, its diameter. This investigation has been performed at the atomistic level, and we employed the YASP[37] MD code. All simulations were carried out at a pressure of 101.3 kPa and a temperature of 590 K. The temperature is above the glass-transition temperature of polystyrene of 368 K. These simulation conditions enabled us to understand the structural properties of a polymer melt in the vicinity of a silica spherical surface. The important topic of the polymer dynamics in the vicinity of the surface is intended to be a part of our forthcoming work. The nanoparticle is either ungrafted (bare) or grafted with a-PS chains of the same length as the matrix chains. Two grafting densities have been chosen. All polymer chains consist of 20 monomers. The grafted chains are covalently attached to the spherical silica nanoparticle by an anionic linker unit. Our investigation intends to give insight into the effect of surface curvature and grafting densities on the structure of the surrounding polymer, the possible formation of an interphase, and the interpenetration of grafted and free polystyrene chains. This information will serve as input to the rational design of well-dispersed nanoparticles because this determines the nanocomposite material properties.[38] A second purpose of this work is to provide reference data for the generation of a coarse-grained model of polystyrene-silica nanocomposites, which will allow for the simulation of larger systems containing longer polymer chains.

2. MODEL AND SIMULATION DETAILS

MD simulations were performed of a-PS ($-[C_8H_8]-_n$) in contact with either an ungrafted or an a-PS-grafted spherical silica (SiO_2) nanoparticle. Nanoparticle diameters of 3, 4, and 5 nm as well as grafting densities of 0.0 (bare, ungrafted), 0.5, and 1.0 chains/nm^2 were simulated. Because of the large computational demand to equilibrate long polymer chains, both free and grafted a-PS chains in our model system have been restricted to n = 20 monomers. All polymer chains have been terminated by a methyl group ($-CH_3$). Grafted a-PS chains were attached to the silica surface oxygen atoms via an anionic linker unit/molecule ($-[H_2C(H(C_2H_3)C]_3(CH_3)_2Si-$), as used in experiments.[39] A picture of this molecule is shown in the Supporting Information in Figure SI-18.

The systems studied by atomistic MD simulations are summarized in Table 1. The total number of grafted and free chains was at least 202. Despite an increasing mass (or volume) fraction of the silica nanoparticle with increasing diameter, the obtained results can be systematically deduced across the different systems. The basis for comparison among the different systems containing different nanoparticle sizes is the grafting density, ρ_{gr}. The bulk mass density of a-PS was 910.86 ± 1.52 kg/m^3 at 590 K and 101.3 kPa (experimental[40] density = 904.02 ± 0.10 kg/m^3). The average mass density of the silica nanoparticle was 2770.60 ± 7.56 kg/m^3 (density of natural quartz[41] = 2635−2660 kg/m^3).

Tables 2−5 provide a summary of the potential energy parameters. Force field parameters (containing the Lennard-Jones and Coulombic terms) for a-PS have been designed to describe mixtures of a-PS with benzene[42] and ethylbenzene.[43] They are based on the OPLS-AA force field[44] for hydrocarbon systems. The same force-field parameters were used for the anionic linker molecule. Harmonic dihedral angles were employed for the carbon−carbon double bonds in the linker

Table 2. Nonbonded Force-Field Parameters for Atactic-Polystyrene and Silica[a]

Nonbonded interactions	$V(r_{ij}) = 4\varepsilon[(\sigma/r_{ij})^{12}-(\sigma/r_{ij})^{6}] + (q_iq_j/4\pi\varepsilon_0 r_{ij})[r_{ij}^{-1}+((\varepsilon_{RF}-1)(2\varepsilon_{RF}+1))(r_{ij}^{2}/r_{cutoff}^{3})]$		
	ε/kJ mol^{-1}	σ/nm	q/e
polystyrene			
Csp^3	0.3519	0.3207	0.000
Hsp^3	0.3180	0.2318	0.000
Csp^2	0.2940	0.3550	−0.115
Csp^2	0.2940	0.3550	0.000
Hsp^2	0.1260	0.2420	0.115
anionic linker molecule			
Csp^3	0.3519	0.3207	0.000
Hsp^3	0.3180	0.2318	0.000
C2sp^2	0.3180	0.3550	−0.230
C1sp^2	0.3180	0.3550	−0.115
Hsp^2	0.1260	0.2420	0.115
Si[b]	2.5104	0.3920	0.255
silica nanoparticle			
Si[b]	2.5104	0.3920	1.020
O[b]	0.6368	0.3154	−0.510
H[b]	0.0920	0.2352	0.255

[a] Nonbonded interactions are considered between all atom pairs that are more than two bonds apart, that is, pairs whose distance is not fixed by connectivity. The first part of the nonbonded potential, $V(r_{ij})$, is a Lennard-Jones potential determined by the interaction energy, ε, and the contact distance, σ. The second part is a Coulomb potential between two charges q_i and q_j. The vacuum permittivity is denoted as ε_0. The effect of a reaction field with a dielectric constant ε_{RF} beyond the cutoff is modeled by a Kirkwood approximation. Lennard-Jones parameters for mixed interactions are obtained from the Lorentz−Berthelot mixing rules.[46] For the Lennard-Jones part of the potential, a long-range correction to the virial is applied. The labels sp^2 and sp^3 denote carbon atoms with three and four covalent bonds, respectively. Hydrogen atoms covalently attached to sp^3 hybridized carbon atoms are also labeled with the abbreviation sp^3, that is, Hsp^3. C1sp^2 and C2sp^2 are the first and second carbon atoms in the vinyl group that branches from the backbone of the anionic linker molecule. [b] Silica core parameters were obtained from ref 45. The rest of the parameters are based on the OPLS-AA force field.[44]

Table 3. Bond Stretching Potentials[a]

bonds	$V_{bond} = (k_r/2)(r - r_0)^2$	
	r_0/nm	k_r/kJ mol^{-1} nm^{-2}
polystyrene		
Csp^3−Csp^3	0.153	259 780[b]
Csp^3−Hsp^3	0.109	200 000[b]
Csp^2−Csp^2	0.139	393 022[b]
Csp^2−Hsp^2	0.108	200 000[b]
Csp^3−Csp^2	0.151	265 646[b]
anionic linker molecule		
Csp^3−Csp^3	0.153	259 780[b]
Csp^3−Hsp^3	0.109	200 000[b]
Csp^3−Csp^2	0.151	265 646[b]
C1sp^2−Hsp^2	0.108	313 355
C2sp^2−Hsp^2	0.108	313 355
C1sp^2−C2sp^2	0.134	547 460
Csp^3−Si	0.184	100 000
Si−O	0.163	323 984[c]
silica nanoparticle		
Si−O	0.163	323 984[c]
O−H	0.095	533 549[c]

[a] For explanations of the symbols, see Table 2. Differences in the magnitude of force constants arise from the use of different empirical force fields. [b] Refs 47−49. [c] Ref 50.

molecule and the phenyl rings to maintain planarity. Carbon and hydrogen atoms of the phenyl ring have small partial charges to reproduce the electric quadrupole moment. Silica Lennard-Jones and Coulombic interaction parameters were obtained from a model that describes bulk crystalline silica.[45] In this force field, silicon and oxygen atoms have partial charges. Surface silica oxygen atoms were saturated with hydrogen atoms. No torsional potentials are necessary inside the spherical silica core.

The MD simulation code, YASP,[37] was used at constant temperature T and pressure P, employing Berendsen's thermostat weak coupling[53] to a temperature bath of 590 K and a pressure bath of 101.3 kPa. The coupling times were 0.2 (T) and 0.5 ps (P), whereas a time step of 1 fs was employed. A cutoff radius of 1.0 nm was employed for the nonbonded interactions and a reaction-field correction for the Coulombic[37] interactions. An average effective dielectric constant of the continuum ε_{RF} of 3.7 (experimental dielectric constant: 2.4 to 2.7 for amorphous PS and 4.4 to 4.6 for amorphous silica at room temperature)[41] was assumed. An atomic Verlet neighbor list with a cutoff radius of 1.1 nm was used and updated every 15 time steps. Simulation configurations were sampled every 2000 time steps (2 ps).

A similar procedure to that used by Qian et al.[43] was utilized to create the initial configuration of the polystyrene chains. Fully stretched (all *trans*-) polystyrene chains were initially made by replicating two different types of monomers having different absolute configurations (stereochemistry). A uniform random number controlled the resulting stereochemistry of each monomer,

dx.doi.org/10.1021/ma102833u |*Macromolecules* 2011, 44, 2316–2327

Table 4. Bond Angle Potentials[a]

bond angles	$V(\theta) = (k_\theta/2)(\theta - \theta_0)^2$ θ_0/degrees	k_θ/ kJ mol^{-1} rad^{-2}
polystyrene		
Hsp^3−Csp^3−Hsp^3	109.45	306.40
Csp^3−Csp^3−Hsp^3	109.45	366.90
Csp^2−Csp^3−Csp^3	109.45	366.90
Csp^3−Csp^3−Csp^2	109.45	482.30
Csp^3−Csp^3−Csp^3	109.45	482.30
Csp^3−Csp^2−Csp^2	120.00	376.60
Csp^2−Csp^2−Csp^2	120.00	376.60
Csp^2−Csp^2−Hsp^2	120.00	418.80
anionic linker molecule		
Hsp^2−C1sp^2−C2sp^2	120.00	366.90
Hsp^2−C2sp^2−C1sp^2	120.00	366.90
Csp^3−C1sp^2−Hsp^2	120.00	366.90
Csp^3−Csp^3−Csp^3	109.45	482.30
Csp^3−C1sp^2−C2sp^2	120.00	376.60
Csp^3−Csp^3−Hsp^3	109.45	366.90
Hsp^3−Csp^3−Hsp^3	109.45	306.40
Hsp^3−Csp^3−Si	109.45	482.30
Csp^2−Csp^3−Si	109.45	482.30
Csp^3−Si−Csp^3	109.45	482.30
O−Si−Csp^3	109.47	469.72
Hsp^2−C2sp^2−Hsp^2	120.00	272.80[b]
silica nanoparticle		
Si−O−Si	144.00	209.60[c]
Si−O−H	119.52	228.84[d]
O−Si−O	109.47	469.72[d]

[a] For explanations of the symbols, see Table 2. [b] Ref 51. [c] Ref 52. [d] Ref 50.

Table 5. Dihedral Angle Potentials[a]

dihedral angles	$V(\varphi) = (k_\varphi/2)[1 - \cos m(\varphi - \varphi_0)]$ φ_0/degrees (m, multiplicity)	k_φ/ kJ mol^{-1}
polystyrene		
Csp^3−Csp^3−Csp^3−Csp^3	180.0 (3)	12.0
Csp^3−Csp^3−Csp^3−Hsp^3	180.0 (3)	12.0 (terminal methyl group)
anionic linker molecule		
Csp^3−C1sp^2−C2sp^2−Hsp^2	180.0 (2)	12.0
C2sp^2−C1sp^2−Csp^3−Hsp^3	180.0 (3)	12.0
Csp^3−Csp^3−Csp^3−Csp^3	180.0 (3)	12.0
Csp^3−Csp^3−Csp^3−Si	180.0 (3)	12.0
Csp^3−Csp^3−Si−O	180.0 (3)	12.0
O−Si−Csp^3−Hsp^3	180.0 (3)	12.0
Csp^3−Si−O−Si	180.0 (3)	12.0

harmonic dihedral angles	$V(\varphi) = (k_\varphi/2)(\varphi - \varphi_0)^2$ φ_0/degrees	k_φ/ kJ mol^{-1}rad^{-2}
polystyrene		
Csp^2−Csp^2−Csp^2−Csp^2	0.0	167.4
Csp^2−Csp^2−Csp^2−Hsp^2	0.0	167.4
Csp^2−Csp^2−Csp^2−Csp^3	0.0	167.4
Anionic linker molecule		
Hsp^2−C1sp^2−C2sp^2−Hsp^2	0.0	167.4

[a] For explanations of the symbols, see Table 2.

R and S configuration having equal probabilities. All chains therefore had different stereochemistry. These chains were placed on a lattice inside a cubic periodic simulation cell at a density below 20 kg/m^3. Polymer chains in the center of the box were removed to create a cavity into which the silica nanoparticle was inserted.

The silica core was constructed from a lattice of crystalline silica.[54] To construct a nanoparticle of radius r and a center located at point x, all silicon atoms lying outside this sphere were initially deleted. Second, all oxygen atoms that were not connected to the retained silicon atoms were also removed. This procedure guaranteed that silicon atoms that remained on the surface were saturated by oxygen atoms. All silicon atoms that had bonds with three surface oxygen atoms were deleted to reproduce the crystal structure of α-quartz in the core and in accordance with previous work of Brown et al.[25] In their work dealing with silica surfaces and silica nanoparticles, they observed that a silicon atom can be connected to either one or two silanols (oxygen−hydrogen group) but never to three of them. Third, all remaining surface oxygen atoms were saturated with hydrogen to satisfy their chemical bonding. Charges were chosen to ensure a sum of zero over all nanoparticle atoms. If a silicon atom had been deleted, then the three surface oxygen atoms to which it had been attached were also deleted, whereas the fourth oxygen was saturated with hydrogen. Fourth, to prepare the nanoparticle for the grafting procedure, random points on the surface of a geometrical sphere with radius r and center x were selected using the algorithm of Marsaglia.[55] Finally, because the nanoparticle sphere is not perfect, special care was taken to determine where to connect the grafted chains. For this purpose, hydrogen atoms that had coordinate points located nearest to the random points were deleted and replaced by perfectly stretched a-PS chains. But, note that the grafting to the surface occurs via the anionic linker molecule. After having relaxed the isolated grafted silica nanoparticle, it was finally inserted into the previoulsy created cavity in the midst of the bulk polymer box.

As already mentioned, the density of the initial system configuration was <20 kg/m^3 because the polystyrene chains were well-separated on a lattice to allow for their full relaxation at 490 K for 1 ns. The end-to-end distance autocorrelation function decayed to zero during this time. When the system was compressed under isothermal−isobaric conditions, it took at least 3 ns to reach an equilibrated density at 490 K. Owing to the slow relaxation of polystyrene chains at 490 K, annealing simulations were carried out. The system temperature was increased from 490 to 990 K and simulated at the high temperature for 1 ns. Following this step, it was decreased to 590 K at a rate of 100 K/ns. Equilibration of the systems was performed for a minimum time of 47.6 ns at 590 K (for the final densities, see Table 1) to take advantage of the shorter relaxation time at this temperature compared with 490 K. Production runs were conducted at 590 K for a period of 6 ns while sampling the system configurations every 2000 time steps (2 ps).

3. RESULTS AND DISCUSSION

3.1. Polymer Density around the Nanoparticle. The radial monomer number density of the polystyrene phase is shown in Figure 1. It has been obtained by sorting the centers of mass of the repeat units into spherical bins of thickness 0.05 nm around the silica nanoparticle. Having calculated the center of mass of the silica core in every sampling time unit, the position of the nanoparticle surface was

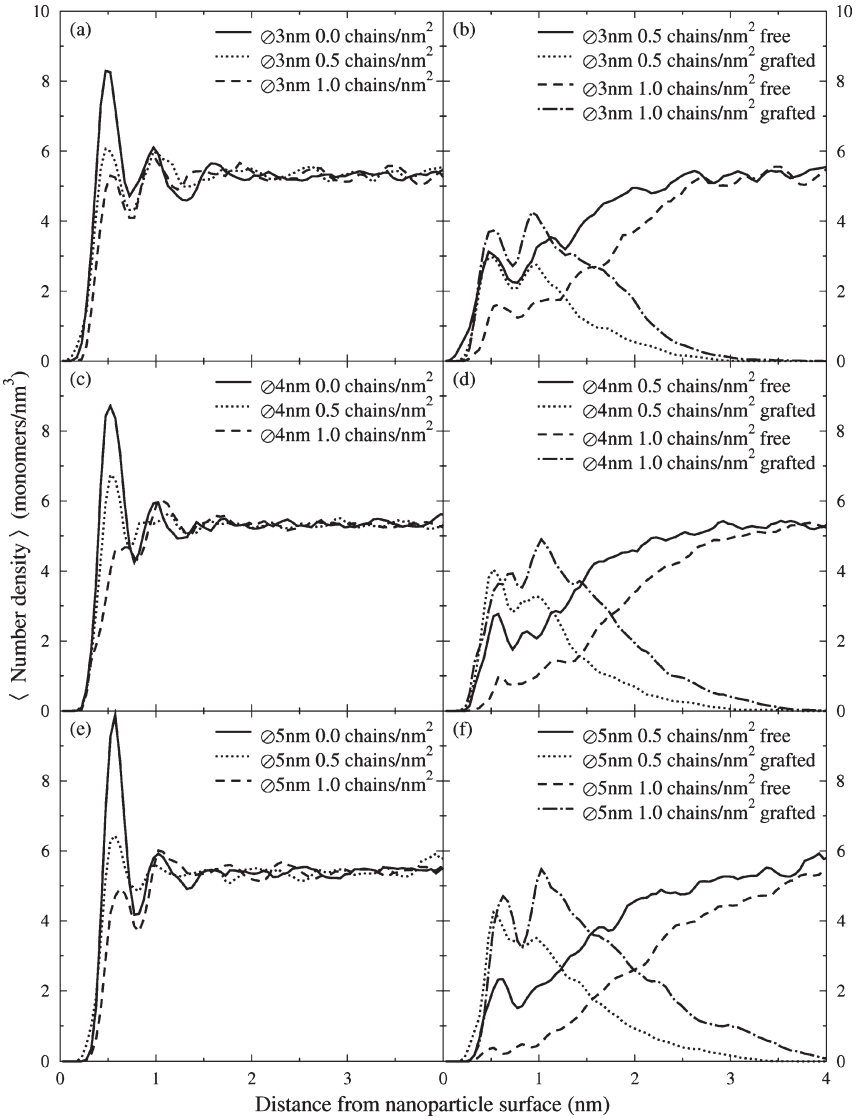

Figure 1. Polystyrene monomer number density as a function of the radial distance from the silica nanoparticle. Panels (a), (c), and (e) summarize the overall monomer number density profiles (excluding the linker molecule) for the bare (solid line), medium (dotted line), and high grafted particle (dashed line) systems as a function of the nanoparticle diameter. Panels (b), (d), and (f) show the separated monomer number density profiles of grafted and free chains. The simulations have been performed at T = 590 K and P = 101.3 kPa.

defined to be at the selected radius of the nanoparticle (1.5, 2.0, or 2.5 nm). Silica and linker atoms were not included in the density analysis. (Note that equivalent graphs of the polymer atomic mass densities show essentially the same behavior, but here the features are less well-defined. For this reason, the mass density profiles are included in the Supporting Information (SI) as Figure SI-1.) In all studied systems, the polymer chains form layers[23−26,56−59] around the nanoparticle, evidenced by an oscillating density profile, Figure 1a,c,e. At least two maxima are visible at 0.5 and ∼1.0 nm from the surface. The first peak exceeds the bulk monomer and mass densities by at least a factor of 1.4; overall monomer number density profiles even show a factor of 1.9 in Figure 1e. This behavior is similar to the density profile of a fluid that wets a surface reasonably well.[60] The density amplitudes around a bare (ungrafted) nanoparticle increase with the diameter of the nanoparticle: the height of the first peak, for example, is 8.3, 8.7, and 9.9 monomers/nm^3 for particles of 3, 4, and 5 nm, respectively. This is easily understood from geometric arguments: a flatter surface (larger particle diameter) allows the monomers less lateral leeway and has a stronger ordering effect. This will be a recurring theme in the discussions below.

The density amplitudes decrease with increasing grafting density. For all particle diameters, the polymer chains in the ungrafted systems have the largest density oscillations, followed by those surrounding a grafted particle with grafting densities of 0.5 and then 1.0 chains/nm^2. The reason here is presumably that the presence of chemically grafted chains on the surface prevents, to differing extents, free chains from adsorbing flat onto the surface and thereby forming discrete layers. Grafted chains themselves, however, contribute to discernible monomer density maxima around the nanoparticles, as illustrated in Figure 1b,d,f. The tendency for grafted chains to stretch away from the surface increases with increasing grafting density and particle diameter because the grafted chains become more constrained by their neighbors and are forced to extend more. The grafted chains also inhibit the approach of the free chains to the nanoparticle. This is shown in Figure 1b,d,f as well as in the mass density profiles (Figure SI-1b,d,f of the Supporting Information). The strength of the

dx.doi.org/10.1021/ma102833u |*Macromolecules* 2011, 44, 2316–2327

Table 6. Density Crossover Distance, r_{co} (nanometers)[a]

nanoparticle diameter ∅ (nm)	grafting density (0.5 chains/nm^2)	grafting density (1.0 chains/nm^2)
	r_{co}/nm	r_{co}/nm
3	0.825 ± 0.025	1.575 ± 0.025
4	1.125 ± 0.025	1.775 ± 0.025
5	1.225 ± 0.025	1.975 ± 0.025

[a] Below the indicated distances from the nanoparticle surface, the monomer density of the grafted chains exceeds that of the free chains. Above r_{co}, the monomer density contribution of the free chains is larger. The magnitude of the error (±0.025) is equal to half the bin width used in the density calculation.

repulsion increases again with increasing particle diameter and grafting density. A larger particle diameter leads to a lower surface curvature and less space between the protruding grafted chains. This observation is consistent with the prevailing notion that more curvature tends to increase the interpenetration between the free and the grafted chains.[36] Because grafted chains dominate the interfacial region, the free chains have a smaller contribution towards the first peak that was observed near bare nanoparticles and this only significantly occurs at the lower grafting density of 0.5 chains/nm^2. At the higher grafting density of 1.0 chains/nm^2, the concentration of monomers of free chains near the surface is too low to show any ordered structure.

There is convergence in the overall density profiles toward the bulk density value at a distance of ∼2.0 nm away from the nanoparticle surface for all systems (Figure 1a,c,e). This distance happens to be close to twice the radius of gyration for the studied polymers (free chains). In view of the short chain lengths, it is not clear whether there is a systematic reason or whether this is mere coincidence. However, it is interesting that this observation seems to be reproduced in experimental[61] work that employs longer chains and larger nanoparticles.

Figure 1b,d,f shows that the decomposed monomer density profiles take longer to converge than the overall density. There is a small fraction of grafted monomers still found at distances of ∼2.5 nm from the surface. This effect is enhanced with increasing diameter and grafting density. Simultaneously, monomers of free polymer chains can be found within 0.5 nm away from the surface in all studied systems, that is, well inside the grafted brushes. This observation is evidence that the free polymer chains are able to penetrate and mix with the grafted polymer chains. Furthermore, the shape of the grafted polymer chains density profiles shown in Figure 1b,d,f is similar to that of previous work reported by Borukhov and Leibler[19] of wet brushes, in which grafted chains mix well with free chains. Compared with the idealized step function[62,63] or parabolic[64] approximation for the polymer brush density, the present MD results are more realistic and similar to experimental observations. The stretched-out conformations of grafted chains in this MD simulation study for a grafting density of 1.0 chains/nm^2 is similar to chains appearing in the "concentrated" regime that has been described in the experimental work of Dukes et al.[65] The collapsing of chains onto the surface under lower grafting density conditions (0.5 chains/nm^2) resembles conformations in what they call the "semidilute" regime.

Decreasing surface curvature and increasing grafting density both have the effect of extending the reach of the grafted chains. Consequently, the ability of free chains to approach the surface is reduced. A good measure to describe the extension of the interphase of different systems is the crossover distance, r_{co}, that is, the point beyond which the density contribution of the free chains is larger than that of the grafted chains (Table 6). Clearly, the effect of surface curvature and grafting density is that r_{co} shifts away from the nanoparticle surface, even by as much as 0.7 nm when doubling the grafting density. It shifts by at least 0.1 to 0.3 nm when reducing the nanoparticle surface curvature. Again, a recurring observation is that high nanoparticle surface curvature is associated with increased interpenetration between grafted and free chains. This effect is vital in creating well-dispersed grafted nanoparticles in a polymeric matrix. A caveat: whereas the crossover distance is one measure of the interphase width, the interphase terminates only when there are no more grafted monomers. This happens at a distance of about 1.9 to 3.6 r_{co} (Figure 1b,d,f).

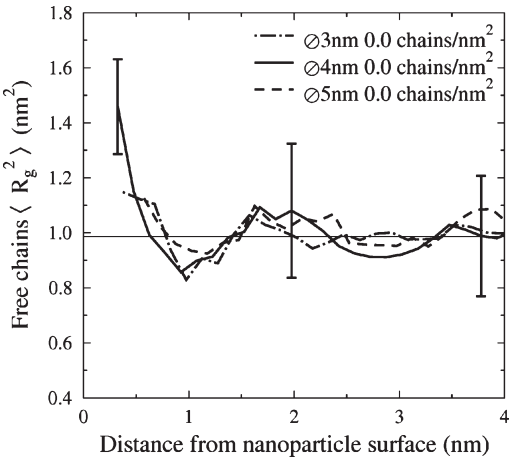

Figure 2. Squared radius of gyration of free polymer chains in the vicinity of a bare nanoparticle. The distance measures the separation of the center of mass of the respective chain from the nanoparticle surface. The horizontal line indicates the squared radius of gyration of free chains (∼1.0 nm^2) in the bulk determined for a polymer system without nanoparticles. For clarity of the diagram, representative error bars are shown (here and in the Figures to follow).

3.2. Chain Extension and Orientation. It is interesting to find out if and how the global chain conformation is affected by the distance of the chain (center-of-mass) from the nanoparticle surface. Figure 2 shows the variation of the squared radius of gyration $\langle R_g^2 \rangle$ of free chains around a bare nanoparticle of different diameters. The profiles are rather independent of the nanoparticle curvature. Polymer chains that are very close to the surface (<0.5 nm) tend to stretch, as also observed by Starr et al.[57] Their $\langle R_g^2 \rangle$ is by a factor of about 1.1 to 1.4 times larger than the bulk value of ∼1.0 nm^2 (labeled by the horizontal line). The reference value of 0.986 ± 0.060 nm^2 was calculated from a simulation of only bulk a-PS. This region is followed by a shallow minimum (∼0.5 to ∼1.0 nm) in all curves. In consideration of the error bars, it is difficult to say if it is a real feature or an artifact of bad statistics. Beyond 1.0 to 1.3 nm, the squared radius of gyration approaches bulk behavior. Hence, the interphase

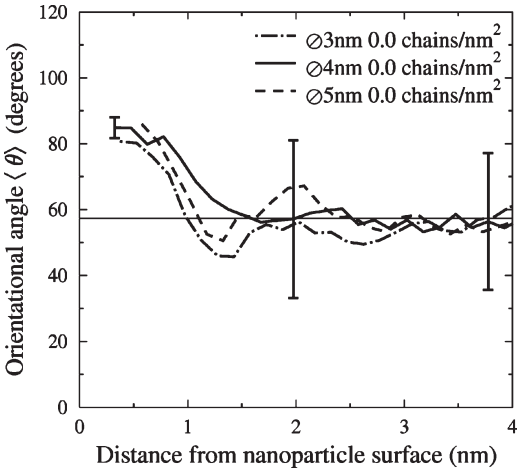

Figure 3. Chain orientation as a function of the chain (center-of-mass) distance from the nanoparticle surface for ungrafted systems. The considered nanoparticle diameters were 3, 4, and 5 nm. The orientation angle is calculated between the longest axis of the squared radius of gyration tensor (eigenvector corresponding to its largest eigenvalue, disregarding the sign) and the surface normal. The horizontal line at 57.3° marks the average orientational angle for a random distribution.

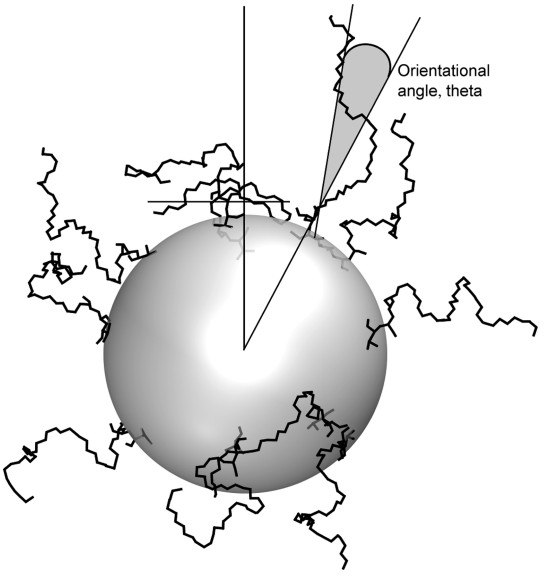

Figure 4. Schematic representation of the orientational angle θ between the longest axis of the squared radius of gyration tensor and the surface normal (simulation snapshot).

thickness, as measured by peculiarities of the chain extension, is of this order of magnitude. The presence of the surface also influences the orientation of the chains. Figure 3 shows the distance dependence of the angle between the longest axis of the squared radius of gyration tensor and the surface normal of the bare nanoparticle. The observation that the free polymer chains generally prefer to align tangentially to the ungrafted surface is in agreement with conclusions from other researchers.[23,66] In their coarse-grained model using Monte Carlo simulations, Vogiatzis et al.[23] studied the orientational angles of local chain segments. They also concluded that chain segments in the vicinity of the nanoparticle surface were structured and oriented tangentially to the interface.

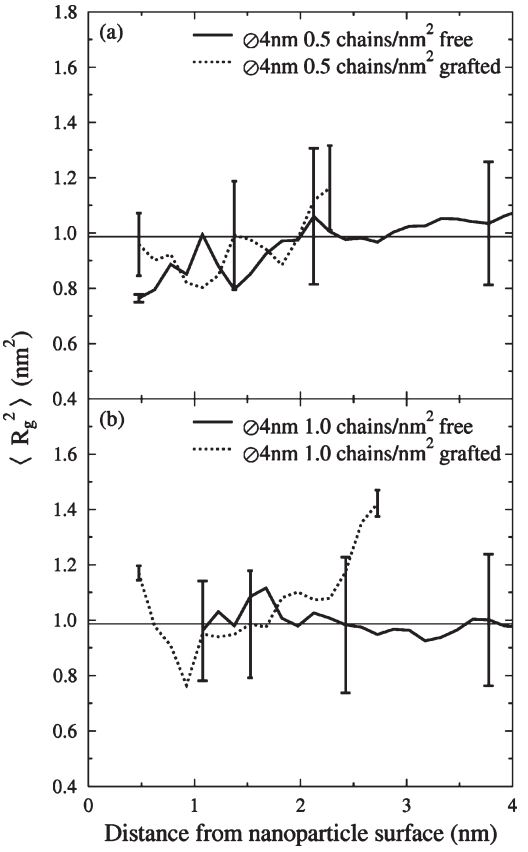

Figure 5. Squared radius of gyration of grafted and free chains around a grafted nanoparticle of diameter 4 nm as a function of the distance of their centers of mass from the nanoparticle surface and the grafting density. The horizontal line indicates the squared radius of gyration of free chains (~1.0 nm^2) in the bulk.

The orientational angle θ for grafted chains is shown schematically in Figure 4. The same definition is applied to the free chains as well. These simulations confirm that the stretching of chains very close to the surface (<0.5 nm) implies a chain orientation that is tangential to the surface. This is predictable because chains have to be compressed flat against the surface if they are to approach it closely. This orientational preference decreases steadily to approach the expected bulk average[67−69] of 57.3° at 1.0 to 1.2 nm. The orientational order, thus persists to a similar distance from the surface as the chain extension when measured by the mean-squared radius of gyration. (See above.)

The behavior of free chains does not change qualitatively, when the system is switched from a bare to a grafted nanoparticle. Figures 5 and 6 present the squared radius of gyration and orientational angles for systems with a nanoparticle of 4 nm diameter and different grafting densities as an example. (The full set of curves is found in Figures SI-2−SI-9 in the Supporting Information.) Taking into consideration the error bars and looking at all distributions (Figures SI-2−SI-5 of the Supporting Information), one finds that the free chains have a bulk-like $\langle R_g^2 \rangle$, regardless of their separation from the nanoparticle surface. They do not stretch significantly. However, combining Figures 5a and 6a showing data for $\rho_{gr} = 0.5$ chains/nm^2, we observe that the free chains still orient tangentially to the surface despite the absence of stretching. This implies that tangential orientation to the surface normal vector is not restricted to fully stretched-out chains but that it can also be brought about, for example, by flat chains having pancake shapes. In contrast, free chains nearest to the nanoparticle

dx.doi.org/10.1021/ma102833u |*Macromolecules* 2011, 44, 2316–2327

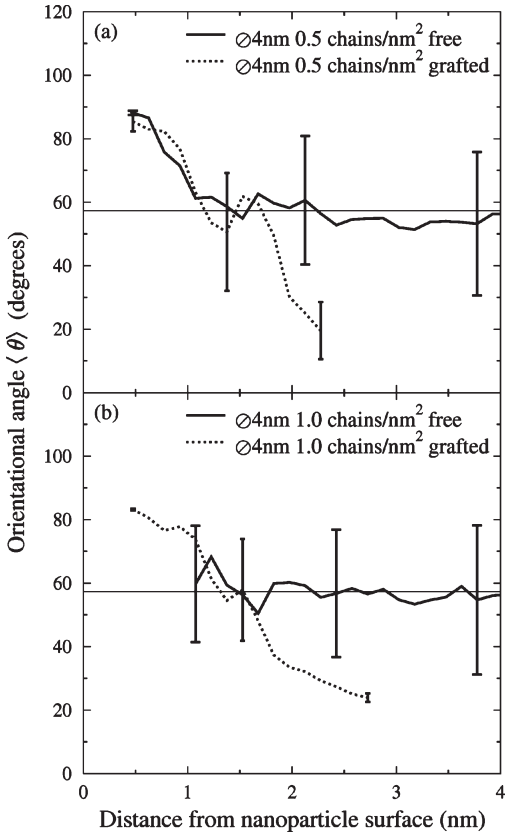

Figure 6. Chain orientational angles as a function of the chain (center-of-mass) separation from the surface for systems containing a nanoparticle of 4 nm diameter and grafted densities 0.5 and 1.0 chains/nm^2. The orientational angle is calculated between the longest axis of the squared radius of gyration tensor (eigenvalue corresponding to its largest eigenvalue, disregarding the sign) and the surface normal. The horizontal line at 57.3° marks the average orientational angle for a random distribution.

surface in the high grafting density systems mostly have random orientational angles (Figures SI-7−SI-9c of the Supporting Information). These observations are consistent with a picture of the nanoparticle plus its corona of grafted chains acting as an orienter for the free chains. Grafted chains in the lower ρ_{gr} range intermingle more with the matrix chains (so the overall density converges quickly, cf. Section 3.1). The free chains close to the surface also orient tangentially. This influence of grafted chains diminishes beyond a separation of 1.0 nm from the surface where the random orientation of free chains begins. At larger ρ_{gr}, free chains have a reduced ability to penetrate, and the majority of them lie in the fringes of the grafted chains extension area where they are randomly oriented. However, in some cases, the free chains that have penetrated the highly dense grafted chains regime are also tangentially oriented, and in this case, the grafted chains behave as orienters (Figures SI-7 and SI-9c of the Supporting Information).

The grafted chains show an expected behavior in their extension (Figure 6). If their centers of mass are close to the surface, then they are tangentially oriented. For quite a narrow intermediate region, a random orientation ($\theta = 57.3°$) is observed. At larger separations from the nanoparticle surface, the orientational angle of grafted chains is <57.3°, which implies that they are stretched and asymptotically align with the surface normal. Despite the tangential orientation, grafted chains close to the surface are not always stretched but rather show a bulk-like $\langle R_g^2 \rangle$ for a small ρ_{gr}. However, for grafted chains that have their center of mass close to the surface, their known tendency to stretch is observed only for the larger nanoparticles with reduced curvature (Figures SI-4 and SI-5 of the Supporting Information). Mass centers of grafted chains that are located furthest away from the nanoparticle surface correspond to grafted chains that are both stretched and oriented perpendicular to the surface. These chains have a large squared radius of gyration and a small orientation angle with the surface normal. This is exemplified in Figures 5 and 6 and confirmed for the other systems in the Supporting Information (Figures SI-2−SI-9).

A similar orientational behavior can be observed on a more local scale. We have also calculated the orientational angles of chain segments of one and three monomers. Segment orientations were defined as the unit vector between the backbone carbons carrying the phenyl groups of two adjacent repeat units i and $i + 1$, as well as between repeat unit i and $i + 3$, respectively. The orientational angles are defined, as before, as the angle between this intermonomer vector, disregarding its sign, and the surface normal. The distance of a segment from the surface is calculated from the position of the midpoint of the respective intermonomer vector. Similar orientational behavior of both grafted and free chains is observed for both segment lengths. This is shown in Figure 7 for the nanoparticle with a diameter of 4 nm, whereas the complete data can be found in the Supporting Information (Figures SI-10−SI-17). At very short distances from the surface (0.8 to 1.0 nm), there is, on average, a small preference for a tangential orientation of the segments. Beyond this distance, the segment orientation is random. Note, however, that the error bars are large (30°). We can conclude that the orienting effect of the surface on short stretches of the polymer is small and limited to the immediate neighborhood of the surface. Therefore, no longer-reaching interphase manifests itself in this property.

4. SUMMARY AND CONCLUSIONS

The structure of atactic polystyrene in the immediate neighborhood of a spherical silica nanoparticle with a diameter of 3, 4, and 5 nm has been investigated by MD simulations at the atomistic level. Particular attention has been paid to the influence of the size of the nanoparticle or, equivalently, the curvature of its surface, as well as its grafting state. Ungrafted (bare) nanoparticles as well as a particles grafted with polystyrene chains at grafting densities of 0.5 and 1.0 chains per nm^2 surface area were studied. Grafting densities in this range are frequently employed in experimental work[61] to facilitate the dispersion of nanoparticles in the polymer.

The nanoparticle has a structuring influence on the polymer in its vicinity. This is easily visible in all quantities analyzed. Studied nanoparticles of all diameters and surface decorations induce: (i) layering of monomers, visible in oscillations of the radial monomer number density; (ii) chain extension, visible in an increase in the squared radius of gyration of the chains; and (iii) chain orientation, visible in the orientation of the longest axis of the gyration tensor being tangential to the surface. The quantitative extent of structural modifications of the polymer and their distance range, however, depends on the curvature and grafting state of the nanoparticle. A flatter surface (larger nanoparticle diameter) induces more structure than a more curved one. The reason is geometric: the volume above a circular surface area of a given size is a truncated cone. A flatter surface has a narrower opening angle of the cone. Therefore, if the surface is flat, a polymer molecule adsorbed or grafted to the surface has less space and it interferes more with neighboring molecules.

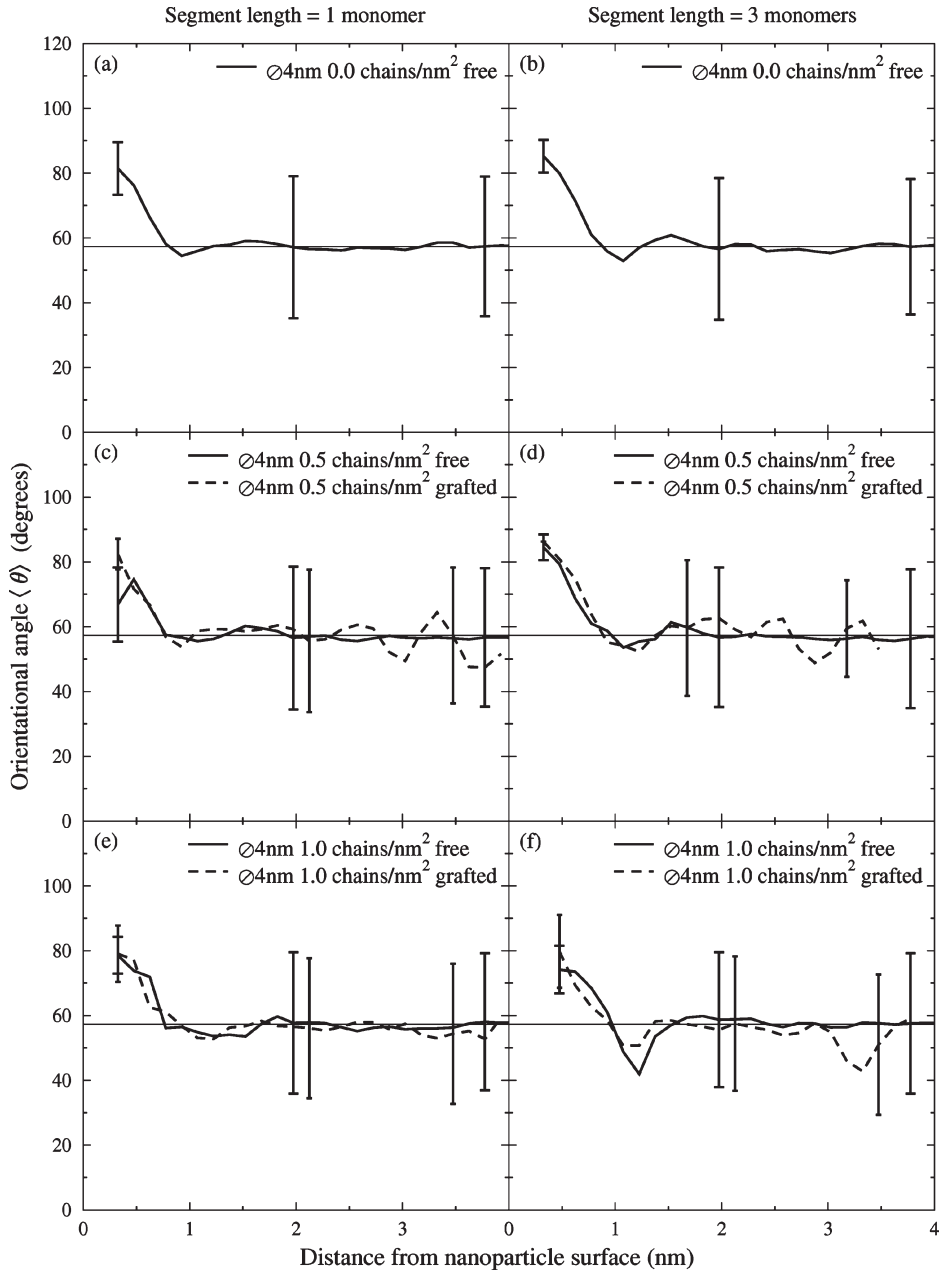

Figure 7. Orientation of chain segments of length 1 (left panels (a), (c), and (e)) and length 3 (right panels (b), (d), and (f)) for a bare nanoparticle (top row of panels (a) and (b)) and for a nanoparticle of a grafted density of 0.5 chains/nm^2 (center row of panels (c) and (d)) and 1.0 chains/nm^2 (bottom row of panels (e) and (f).

A similar argument holds for the different grafting densities. Grafted chains at low grafting density have enough space to make use of their conformational degrees of freedom. This means that they have conformations that are similar to those of bulk polymers and that they leave enough space on the surface for free chains (matrix chains) to approach the surface, too. At a higher grafting density, grafted chains interfere with their neighbors. This has the effect of reducing the available effective volume for each individual grafted chain. They need to stretch away from the surface, and they exclude the free chains. The effects of curvature and grafting density are additive. Still, it must be noted that different structural properties of the polymer are affected to a different degree. All conformational and orientational properties approach their normal, bulk-like behavior within 0.5 to 1.0 nm from the surface and are nearly independent of the nanoparticle size and decoration. The density oscillations reach about twice as far and are more influenced by the nature of the nanoparticle. The farthest reaching structural element is the concentration of grafted chains. Its influence depends strongly on the nanoparticle size and decoration. Some grafted monomers can be found at 2.5 nm for the most favorable case, in which there is significant interpenetration of grafted and free chains.

At the grafting densities studied here, there are still some free polymers, which intermingle with the grafted chains so that the nanoparticle and polymer are compatibilized. However, there is also evidence for some of the grafted chains to collapse onto the nanoparticle, rather than to entangle with free chains. This is shown in the simulation snapshot in Figure 4 and by chain

dx.doi.org/10.1021/ma102833u |*Macromolecules* 2011, 44, 2316–2327

orientational angles that are almost perpendicular to the surface normal vector in Figure 6. A possible consequence is that the mechanical coupling between silica nanoparticles and the surrounding polystyrene is less strong than expected. This is indeed found in experimental investigations.[70]

■ ASSOCIATED CONTENT

Supporting Information. Additional graphs presenting supporting analysis data. This material is available free of charge via the Internet at http://pubs.acs.org.

■ AUTHOR INFORMATION

Corresponding Author

*E-mail: t.ndoro@theo.chemie.tu-darmstadt.de. Tel: +49 (0)6151 16 2398. Fax: +49 (0)6151 16 6526.

■ ACKNOWLEDGMENT

Financial support from the European Union through the project "NanoModel" under grant number 211778 is gratefully acknowledged. We would like to acknowledge the SPP1369 for providing the computer resources. Helpful technical discussions in developing the analysis programs with Frédéric Leroy and Gustavo Rondina are especially appreciated. We are also thankful for insightful discussions with Kurt Binder and, last but not least, collaborators within the NanoModel project.

■ REFERENCES

(1) Kraus, G. *Reinforcement of Elastomers*; Interscience Publishers: New York, 1965.
(2) Kraus, G. *Angew. Makromol. Chem.* **1977**, *60*, 215–248.
(3) Koenig, J. L. *Acc. Chem. Res.* **1999**, *32*, 1–8.
(4) Zhang, Y.; Ge, S.; Tang, B.; Koga, T.; Rafailovich, M. H.; Sokolov, J. C.; Peiffer, D. G.; Li, Z.; Dias, A. J.; McElrath, K. O.; Lin, M. Y.; Satija, S. K.; Urquhart, S. G.; Ade, H.; Nguyen, D. *Macromolecules* **2001**, *34*, 7056–7065.
(5) Bansal, A.; Yang, H.; Benicewicz, B.; Kumar, S. K.; Schadler, L. S. *J. Polym. Sci., Polym. Phys.* **2006**, *44*, 2944–2950.
(6) Bansal, A.; Yang, H.; Li, C.; Cho, K.; Benicewicz, B.; Kumar, S. K.; Schadler, L. S. *Nat. Mater.* **2005**, *4*, 693–698.
(7) Akcora, P.; Liu, H.; Kumar, S. K.; Moll, J.; Li, Y.; Benicewicz, B. C.; Schadler, L. S.; Acehan, D.; Panagiotopoulos, A. Z.; Pryamitsyn, V.; Ganesan, V.; Ilavsky, J.; Thiyagarajan, P.; Colby, R. H.; Douglas, J. F. *Nat. Mater.* **2009**, *8*, 354–359.
(8) Uyama, Y.; Kato, K.; Ikada, Y. *Adv. Polym. Sci.* **1998**, *137*, 1–39.
(9) *Polymer Adsorption and Dispersion Stability*; Goddard, E., Vincent, B.; Eds.; ACS Symposium Series 240; ACS: Washington, DC, 1984.
(10) Mackay, M. E.; Tuteja, A.; Duxbury, P. M.; Hawker, C. J.; Van Horn, B.; Guan, Z.; Chen, G.; Krishnan, R. S. *Science* **2006**, *311*, 1740–1743.
(11) Raviv, U.; Giasson, S.; Kampf, N.; Gohy, J.-F.; Jérôme, R.; Klein, J. *Nature* **2003**, *425*, 163–165.
(12) Klein, J. *Science* **2009**, *323*, 47–48.
(13) Mackay, M. E.; Dao, T. T.; Tuteja, A.; Ho, D. L.; Van Horn, B.; Kim, H.-C.; Hawker, C. J. *Nat. Mater.* **2003**, *2*, 762–766.
(14) Valentin, J. L.; Mora-Barrantes, I.; Carretero-González, J.; López-Manchado, M. A.; Long, D. R.; Saalwächter, K. *Macromolecules* **2010**, *43*, 334–346.
(15) Tsagaropoulos, G.; Eisenburg, A. *Macromolecules* **1995**, *28*, 396–398.
(16) Chevigny, C.; Gigmes, D.; Bertin, D.; Jestin, J.; Boué, F. *Soft Matter* **2009**, *5*, 3741–3753.
(17) Chevigny, C.; Jestin, J.; Gigmes, D.; Schweins, R.; Di-Cola, E.; Dalmas, F.; Bertin, D.; Boué, F. *Macromolecules* **2010**, *43*, 4833–4837.
(18) Kumar, S. K.; Krishnamoorti, R. *Annu. Rev. Chem. Biomol. Eng.* **2010**, *1*, 37–58.
(19) Borukhov, I.; Leibler, L. *Macromolecules* **2002**, *35*, 5171–5182.
(20) Frischknecht, A. L.; McGarrity, E. S.; Mackay, M. E. *J. Chem. Phys.* **2010**, *132*, 204901–204907.
(21) Hooper, J. B.; Schweizer, K. S. *Macromolecules* **2005**, *38*, 8858–8869.
(22) Hooper, J. B.; Schweizer, K. S. *Macromolecules* **2006**, *39*, 5133–5142.
(23) Vogiatzis, G.; Voyiatzis, E.; Theodorou, D. N. *Eur. Polym. J.* DOI: 10.1016/j.eurpolymj.2010.09.017.
(24) Barbier, D.; Brown, D.; Grillet, A.-C.; Neyertz, S. *Macromolecules* **2004**, *37*, 4695–4710.
(25) Brown, D.; Mélé, P.; Marceau, S.; Albérola, N. D. *Macromolecules* **2003**, *36*, 1395–1406.
(26) Borodin, O.; Smith, G. D.; Bandyopadhyaya, R.; Byutner, O. *Macromolecules* **2003**, *36*, 7873–7883.
(27) Eslami, H.; Müller-Plathe, F. *J. Phys. Chem. B* **2009**, *113*, 5568–5581.
(28) Alaghemandi, M.; Böhm, M. C.; Müller-Plathe, F., submitted for publication.
(29) Grest, G. S. *J. Chem. Phys.* **1996**, *105*, 5532–5542.
(30) Lo Verso, F.; Egorov, S. A.; Milchev, A.; Binder, K. *J. Chem. Phys.* **2010**, *133*, 184901–184910.
(31) Kalb, J.; Dukes, D.; Kumar, S. K.; Hoy, R. S.; Grest, G. S. *Soft Matter* **2010**, *7*, 1418–1425.
(32) Klos, J.; Pakula, T. *J. Chem. Phys.* **2003**, *118*, 1507–1514.
(33) Klos, J.; Pakula, T. *J. Chem. Phys.* **2003**, *118*, 7682–7690.
(34) Klos, J.; Pakula, T. *Macromolecules* **2004**, *37*, 8145–8151.
(35) Cordeiro, R. M.; Zschunke, F.; Müller-Plathe, F. *Macromolecules* **2010**, *43*, 1583–1591.
(36) Trombly, D. M.; Ganesan, V. *J. Chem. Phys.* **2010**, *133*, 154904–154911.
(37) Müller-Plathe, F. *Comput. Phys. Commun.* **1993**, *78*, 77–94.
(38) Vaia, R. A.; Maguire, J. F. *Chem. Mater.* **2007**, *19*, 2736–2751.
(39) Hübner, E.; Allgaier, J.; Meyer, M.; Stellbrink, J.; Pyckhout-Hintzen, W.; Richter, D. *Macromolecules* **2010**, *43*, 856–867.
(40) Höcker, H.; Blake, G. J.; Flory, P. J. *Trans. Faraday Soc.* **1971**, *67*, 2251–2257.
(41) Lide, D. R. *CRC Handbook of Chemistry and Physics*, 74th ed.; CRC Press: Bock Raton, FL, 1993.
(42) Müller-Plathe, F. *Macromolecules* **1996**, *29*, 4782–4791.
(43) Qian, H.-J.; Carbone, P.; Chen, X.; Karimi-Varzaneh, H. A.; Liew, C. C.; Müller-Plathe, F. *Macromolecules* **2008**, *41*, 9919–9929.
(44) Jorgensen, W. L.; Maxwell, D. S.; Tirado-Rives, J. *J. Am. Chem. Soc.* **1996**, *118*, 11225–11236.
(45) Lopes, P. E. M.; Murashov, V.; Tazi, M.; Demchuk, E.; MacKerell, J.; Alexander, D. *J. Phys. Chem. B* **2006**, *110*, 2782–2792.
(46) Allen, M. P.; Tildesley, D. J. *Computer Simulations of Liquids*; Clarendon: Oxford, U.K., 1987.
(47) Algaer, E.; Alaghemandi, M.; Böhm, M. C.; Müller-Plathe, F. *J. Phys. Chem. A* **2009**, *113*, 11487–11494.
(48) Lussetti, E.; Terao, T.; Müller-Plathe, F. *J. Phys. Chem. B* **2007**, *111*, 11516–11523.
(49) Valavala, P. K.; Odegard, G. M. *Rev. Adv. Mater. Sci.* **2005**, *9*, 34–44.
(50) Ermoshin, V.; Smirnov, K. S.; Bougeard, D. *J. Mol. Struct.* **1997**, *410−411*, 371–374.
(51) Blom, C. E.; Altona, C.; Oskam, A. *Mol. Phys.* **1977**, *34*, 177–192.
(52) Newton, M. D. *Phys. Chem. Miner.* **1980**, *6*, 305–312.
(53) Berendsen, H. J. C.; Postma, J. P. M.; van Gunsteren, W. F.; DiNola, A.; Haak, J. R. *J. Chem. Phys.* **1984**, *81*, 3684–3690.
(54) Wells, A. F. *Structural Inorganic Chemistry*; Oxford Science Publications: New York, 1984.
(55) Marsaglia, G. *Ann. Math. Stat* **1972**, *43*, 645–646.

(56) Allegra, G.; Raos, G.; Vacatello, M. *Prog. Polym. Sci.* **2008**, *33*, 683–731.
(57) Starr, F. W.; Schrøder, T. B.; Glotzer, S. C. *Macromolecules* **2002**, *35*, 4481–4492.
(58) Vacatello, M. *Macromolecules* **2001**, *34*, 1946–1952.
(59) Vacatello, M. *Macromol. Theor. Simul.* **2002**, *11*, 757–765.
(60) Bucior, K.; Yelash, L.; Binder, K. *Phys. Rev. E* **2009**, *79*, 031604–031616.
(61) Kim, C. J.; Spehr, T.; Stühn, B. Personal communication, 2010.
(62) Alexander, S. *J. Phys. (Paris)* **1977**, *38*, 977–981.
(63) de Gennes, P. G. *Macromolecules* **1980**, *13*, 1069–1075.
(64) Milner, S. T.; Witten, T. A.; Cates, M. E. *Macromolecules* **1988**, *21*, 2610–2619.
(65) Dukes, D.; Li, Y.; Lewis, S.; Benicewicz, B. C.; Schadler, L. S.; Kumar, S. K. *Macromolecules* **2010**, *43*, 1564–1570.
(66) Brown, D.; Marcadon, V.; Mélé, P.; Albérola, N. D. *Macromolecules* **2008**, *41*, 1499–1511.
(67) Morikawa, E.; Saile, V.; Okudaira, K. K.; Azuma, Y.; Meguro, K.; Harada, Y.; Seki, K.; Hasegawa, S.; Ueno, N. *J. Chem. Phys.* **2000**, *112*, 10476–10481.
(68) Bergström, J. S.; Boyce, M. C. *Macromolecules* **2001**, *34*, 614–626.
(69) Palmer, J. S.; Boyce, M. C. *Acta Biomater.* **2008**, *4*, 597–612.
(70) Harton, S. E.; Kumar, S. K.; Yang, H.; Koga, T.; Hicks, K.; Lee, H.; Mijovic, J.; Liu, M.; Vallery, R. S.; Gidley, D. W. *Macromolecules* **2010**, *43*, 3415–3421.